JACS Au
AN OPEN ACCESS JOURNAL OF THE AMERICAN CHEMICAL SOCIETY

pubs.acs.org/jacsau Letter

Switching Singlet Exciton to Triplet for Efficient Pure Organic Room-Temperature Phosphorescence by Rational Molecular Design

Liangwei Ma, Yiwei Liu, He Tian, and Xiang Ma*

Cite This: *JACS Au* 2023, 3, 1835−1842 Read Online

ACCESS | Metrics & More | Article Recommendations | Supporting Information

ABSTRACT: The design and regulation of phosphors are attractive but challenging because of the spin-forbidden intersystem crossing (ISC) process. Here, a new perspective on the enhancement of the ISC is proposed and demonstrated. Different from current strategies, the ISC yield (Φ_{ISC}) is enhanced by decreasing the fluorescence radiative transition rate constant (k_F) via rational molecular designing rather than boosting the spin−orbit coupling by decorating the molecular skeleton with a heavy atom, heteroatom, or carbonyl. The k_F of the designed molecule in this case is associated with the substituent position of the methoxy group, which alters the distribution of the front orbitals. The $S_0 \rightarrow S_1$ transition of these compounds evolves from a bright state to a dark state gradually with the variation of the substituent position, accompanied by the decrease of k_F and increase of Φ_{ISC}. The fluorescence emission is switched to phosphorescence emission successfully by regulating the k_F. This work provides an alternative strategy to design efficient room-temperature phosphorescence material.

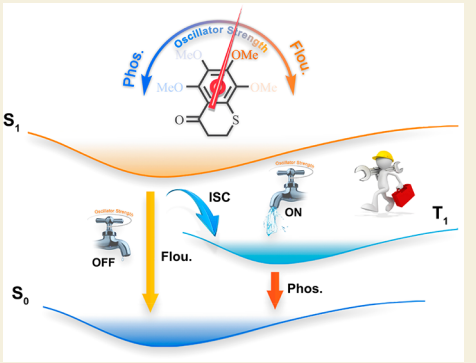

KEYWORDS: *room-temperature phosphorescence, dark state, heavy-atom-free, phosphorescence quantum yield*

Metal-free room-temperature phosphorescence (RTP) materials have received huge research interest because of their unique photophysical properties, like large Stokes-shift, long luminescence lifetime, and triplet-state-involved transition.[1−5] These materials have shown great potential in various fields.[2,5−11] Weak spin−orbit coupling (SOC) and the vulnerable nature of the triplet excited state are the principal difficulties in the design of metal-free RTP materials.[12−16] Great efforts have been made in the past decade to solve these problems.[17−22] Generally, these strategies could be classified into two kinds: (1) inhibiting the nonradiative transition and (2) populating a triplet state exciton. The most popular and efficient strategies to suppress the nonradiative transition have been the embedding of RTP materials into a rigid matrix (micromolecule or polymer), crystallization, and being included in macrocyclic molecules, while the heavy atom (Br, I) effect, heteroatom (N, O, S, B, P) effect, and carbonyl have been the familiar strategies since the 1940s in the facilitation of the intersystem crossing (ISC), which is critical to the population of a triplet state exciton, through enhancement of the SOC.[23] Moreover, H-aggregates, exciplex, cluster-triggered emission, and energy transfer strategies have also been developed to design RTP materials.[21,24,25] By comprehensively utilizing these strategies, many impressive breakthroughs have been made very recently.[13,26,27] For example, the emission wavelength of organic RTP material was up to 819 nm.[28] The phosphorescence quantum yield was enhanced to an extremely high level.[29] The duration time of the afterglow was prolonged to more than an hour.[16]

How to design an efficient phosphor and regulate its performance is one of the most important things in the development of RTP materials. Different from pure organic phosphor, fluorescent dyes have been well investigated in their mechanism, design strategy, and application.[30−36] Phosphorescence emission could be regarded as the twin of fluorescence emission. They are the different results of the same photophysics process.[37] Therefore, utilizing the backbone of a fluorescent dye as the foundation structure to explore new phosphorescent dyes is a feasible strategy in the design of RTP materials.[38−42] How to switch the singlet exciton to a triplet exciton is the key factor of the strategy. In most of the current work, the singlet exciton was switched to a triplet exciton by introducing heavy atom or carbonyl functional groups, which enhanced the ISC by boosting SOC, into the backbone of a fluorescent dye.[20,27,40,43,44] However, a strong SOC does not always hint at an efficient phosphorescence emission. A large energy difference between the lowest singlet excited state (S_1) and triplet state or a high fluorescence radiative transition rate constant (k_F) may break down the superiority of ISC and lead to a small ISC yield (Φ_{ISC}) and phosphorescence quantum

Received: May 30, 2023
Revised: July 4, 2023
Accepted: July 5, 2023
Published: July 7, 2023

https://doi.org/10.1021/jacsau.3c00268
JACS Au 2023, 3, 1835−1842

yield (Φ_P). A new design strategy for efficient RTP materials is in high demand.

Herein, we present a case that switched the fluorescence to phosphorescence efficiently by decreasing the k_F by simply altering the substituent position of methoxyl, which was associated with the energy level of the n orbital. In this case, the n orbital energy of methoxyl-substituted thiochroman-4-one derivatives decreased gradually with the variation of substituent position (Figure 1, **MeTO-1**, **MeTO-2**, **MeTO-3**, and **MeTO-4**), which resulted in the n → π^* transition evolving into the dominant orbitals of the $S_0 \rightarrow S_1$ transition. Therefore, the $S_0 \rightarrow S_1$ transition of **MeTO-3** and **MeTO-4** became a dark state because of the forbidden transition process, which led to an extremely small oscillator strength (f) and k_F. Correspondingly, these compounds evolved gradually from fluorescence-dominant (**MeTO-1**) to phosphorescence-dominant (**MeTO-4**) luminescent material. **MeTO-4**, especially, exhibited a 46.8% Φ_P and near 0% fluorescence quantum yield (Φ_F) in the poly(vinyl alcohol) (PVA) matrix. The fluorescence was switched to phosphorescence effectively by simply altering the substituent position. This work indicated that decreasing the k_F should be an alternative strategy to obtain efficient RTP materials.

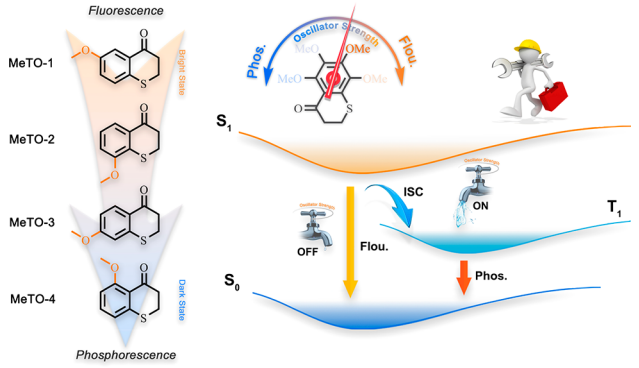

Figure 1. Chemical structure of target compounds and simplified Jablonski diagram for the transition process from the lowest excited state in aromatic compounds.

As shown in Figure 2a, **MeTO-1** exhibited the longest absorption wavelength around 367 nm, tailed to 420 nm, in acetonitrile. An obvious hyperchromatic shift was observed with the variation of substituent position. The 7-substituted thiochroman-4-one derivative (**MeTO-3**) exhibited the shortest absorption wavelength around 330 nm, which was even shorter than thiochroman-4-one.[45] It is worth mentioning that these compounds only exhibit a weak extinction coefficient (~3000 L/mol/cm). Similar to absorption spectra, **MeTO-1** exhibited the longest emission wavelength (448 nm) in the fluorescence spectrum. A 15 nm hyperchromatic shift was observed with the methoxyl changing from the 6- to 8-substituent position (**MeTO-2**). A distinct decrease in intensity was also observed for it. Specifically, Φ_F decreased

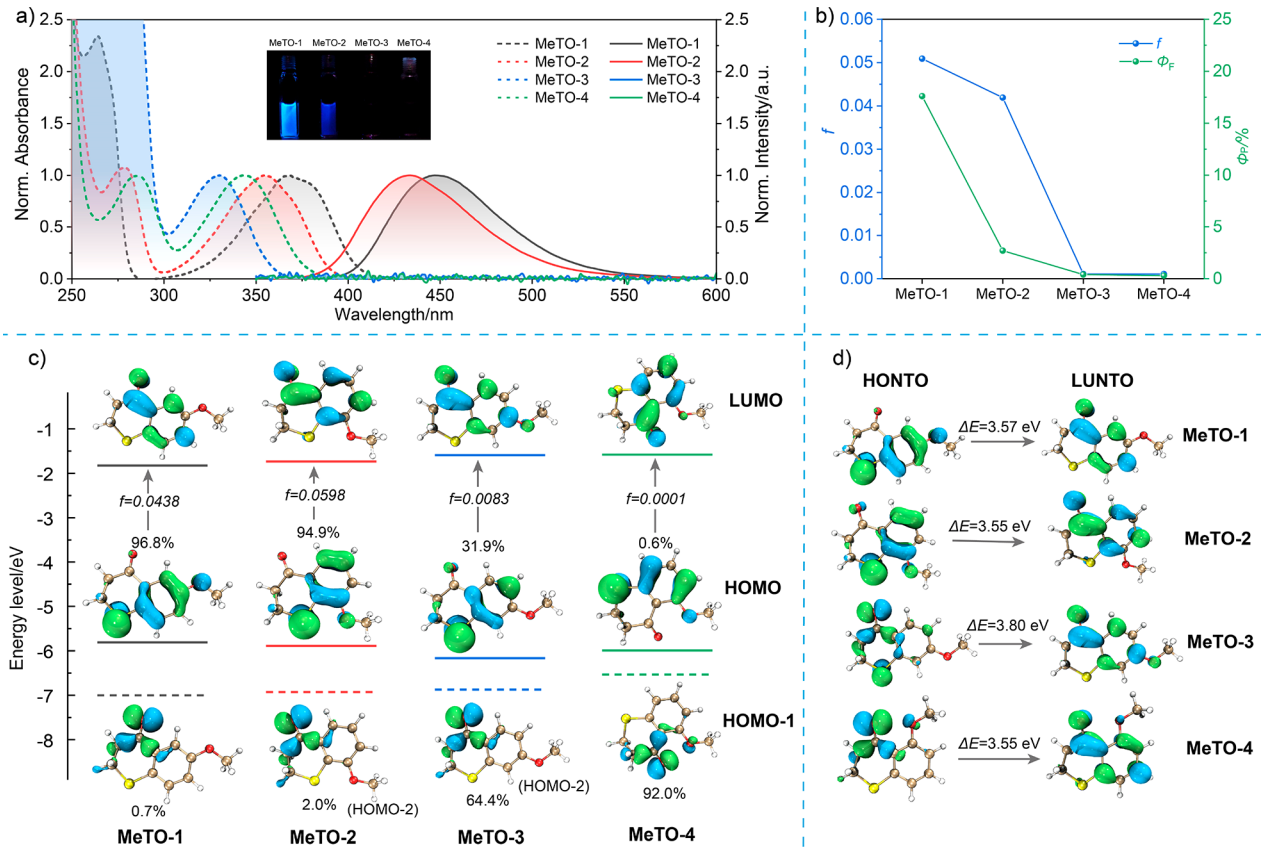

Figure 2. (a) Normalized absorbance (dash line) and fluorescence (solid line) spectra of **MeTOs** in acetonitrile. (b) Calculated f (blue line) and Φ_F of **MeTOs** in acetonitrile; C = 1.0×10^{-4} M. (c) Frontier molecular orbital, energy level diagrams, and transition configurations (%) of $S_0 \rightarrow S_1$ transition of **MeTOs**. (d) highest occupied natural transition orbitals (NTO) (HONTO) and lowest unoccupied NTO (LUNTO) for the $S_0 \rightarrow S_1$ transition of **MeTOs**.

https://doi.org/10.1021/jacsau.3c00268
JACS Au 2023, 3, 1835−1842

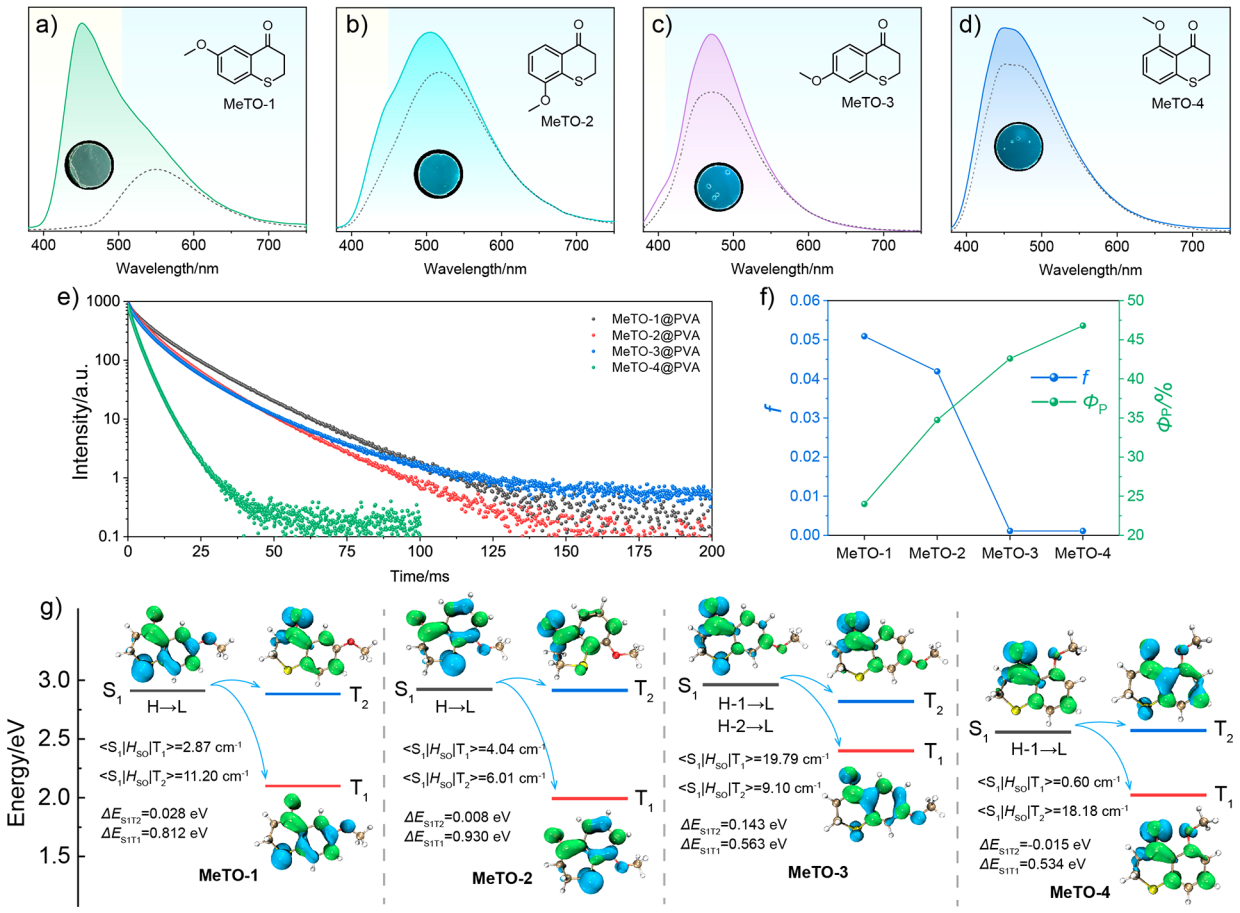

Figure 3. PL (solid line) and phosphorescence (dashed line) spectra of **MeTO-1** (a), **MeTO-2** (b), **MeTO-3** (c), and **MeTO-4** (d) in PVA matrix. (e) Lifetime spectra of phosphorescence emission of **MeTO**s in PVA matrix. (f) The calculated f (blue line) and Φ_P of **MeTO**s in PVA matrix. (g) The frontier molecular orbital, energy level diagrams, and SOC coefficients of **MeTO**s in the gas phase.

from 17.6% to 2.7% (Figure 2b, Table S1), while almost only a noise signal was recorded for the fluorescence spectra of **MeTO-3** and **MeTO-4** (Figure 2a). The absolute quantum yield experiment also agreed with the silence of these compounds in the fluorescence spectrophotometer (Figure 2b, Figure S1). The f was estimated according to the experimental data and listed in Table S1.[46] Interestingly, f decreased from 0.0509 to 0.0011 with the variation of substituent position, thereby indicating that the $S_0 \rightarrow S_1$ transition evolved from a bright state to a dark state gradually, and the Φ_F exhibited the same variation tendency with f (Figure 2b). As listed in Table S1, a distinct decrease was also observed for the k_F. It significantly decreased from 3.74×10^7 s^{-1} to 0.28×10^7 s^{-1} with the variation of substituent position. Such a slow transition process supported the dark state nature of S_1 of **MeTO-3** and **MeTO-4**. In other solvents, these phenomena could also be observed (Figure S3).

To further reveal the possible reason for the dark state, density functional theory (DFT) and time-dependent density functional theory (TD-DFT) calculations were carried out on the Gaussian G09 program at the B3LYP/6-311G* set.[47] As illustrated in Figure 2c, the $S_0 \rightarrow S_1$ transition of all four compounds was assigned to the HOMO/HOMO−1/HOMO−2 → LUMO transition. Because of the very similar molecular skeleton and same electron-withdrawing functional group (carbonyl), the variation of substituent position did not exhibit an obvious influence on the LUMO distribution and energy level. The LUMO of these compounds exhibited a very similar distribution primarily located on the carbonyl and benzene segments, and no obvious variations in the energy level of these LUMOs were observed. However, a significant change was observed in the distribution and energy level of the HOMO, HOMO−1, and HOMO−2 with the variation of the methoxyl group (the electron-donating functional group). The HOMO of **MeTO-1** was located on the sulfur atom and benzene segments, primarily, and assigned to a π-characterized orbit, while the HOMO−1 was primarily located on the carbonyl segments orthogonal with the HOMO and LUMO and assigned to an n-characterized orbital. The $S_0 \rightarrow S_1$ transition of **MeTO-1** was primarily contributed by $\pi \rightarrow \pi^*$ transition (HOMO → LUMO, 96.8%) and partially by an $n \rightarrow \pi^*$ transition (HOMO−1 → LUMO, 0.7%). Moreover, the f of the $S_0 \rightarrow S_1$ transition was calculated to be 0.0483. The HOMO and HOMO−1 distributions of **MeTO-2** were very similar to **MeTO-1**. With variation of the substituent position, a slight decrease in the energy level of the HOMO of the $S_0 \rightarrow S_1$ transition was observed for **MeTO-2**, while the f exhibited a slight increase. Interestingly, the contribution of the $n \rightarrow \pi^*$ transition (HOMO−1 → LUMO, transition forbidden) on the $S_0 \rightarrow S_1$ transition exhibited a slight increase compared with MeTO-1, and a slight decrease was also observed for the contribution of the $\pi \rightarrow \pi^*$ transition (HOMO → LUMO, transition allowed). With the methoxyl changed to the para-position of carbonyl, **MeTO-3** exhibited the lowest HOMO

https://doi.org/10.1021/jacsau.3c00268
JACS Au 2023, 3, 1835−1842

Table 1. Photophysical Parameters of MeTOs in PVA Matrix (0.3 wt %)

	λ_F/nm	λ_P/nm	Φ			τ_F/ns	k_F/s^{-1}[a]	τ_P/ms	k_{ISC}/s^{-1}[b]	Φ_{ISC}/%
			PL/%	phosphorescence/%	fluorescence/%					
MeTO-1	450	550	38.6	24.0	14.6	5.96	2.45×10^7	11.47	1.06×10^8	63.17
MeTO-2	445	517	35.1	34.7	0.4	1.56	0.23×10^7	14.08	6.34×10^8	98.96
MeTO-3		470	42.6	42.6	≈ 0	1.74	≈ 0	11.87	5.75×10^8	99.98
MeTO-4		456	46.8	46.8	≈ 0	0.51	≈ 0	3.60	1.96×10^9	≈100

[a] $k_F = \Phi_F/\tau_F$ [b] $k_{ISC} = \Phi_{ISC}/\tau_F$

energy level, which was calculated to be −6.17 eV. The HOMO−1 → LUMO (n → π^* transition, transition forbidden) transition evolved into the dominant orbitals of the $S_0 \rightarrow S_1$ transition with a 64.4% fraction. Therefore, a small value of f (0.0083) was calculated for it. The f further decreased to 0.0001 with the methoxyl changed to the ortho-position of carbonyl. Similar to the other compounds, the HOMO of **MeTO-4**, located primarily on the sulfur atom and benzene segments, was assigned to the π characteristic orbit. The HOMO−1 located primarily on the carbonyl segments was assigned to the n-characteristic orbit. The $S_0 \rightarrow S_1$ transition of **MeTO-4** was mainly assigned to the HOMO−1 → LUMO (n → π^* transition, 92.0%, transition forbidden) and partially to the HOMO → LUMO ($\pi \rightarrow \pi^*$ transition, 0.6%, transition allowed). The forbidden transition explained the extremely small f of it. It seems that the energy level of the n orbital, distributed on the carbonyl, kept increasing with the variation of substituent position, and the energy level of the π orbit, distributed primarily on sulfur atom and benzene segments, kept decreasing. Therefore, the energy difference between the n and π orbitals kept decreasing. Specifically, the energy difference for **MeTO-1** was calculated to be 1.19 eV, and it decreased to 1.04, 0.71, and 0.54 eV for **MeTO-2**, **MeTO-3**, and **MeTO-4**, respectively. Moreover, the n orbital, located on the carbonyl segments, primarily, evolved into the dominant orbital of the $S_0 \rightarrow S_1$ transition with the variation of the methoxyl substituent position. A clearer picture could be observed in natural transition orbitals (NTO), which were generated by Multiwfn 3.8 program.[48] As illustrated in Figure 2d, the lowest unoccupied NTO (LUNTO) of the four compounds exhibited a very similar distribution, while the highest occupied NTO (HONTO) showed a distinct change with the variation of the substituent position. The HONTO of **MeTO-1** was primarily distributed on the sulfur atom and benzene segments, and a negligible distribution in the carbonyl group was also observed. Interestingly, the distribution of the HONTO changed from the sulfur atom and benzene segments to the carbonyl group gradually with the variation of substituent position, and no obvious distribution of HONTO on the benzene segments was observed for **MeTO-4**, which confirms the forbidden transition nature of the $S_0 \rightarrow S_1$ transition. The $\pi \rightarrow \pi^*$ to n → π^* transition evolution of these compounds should be the inherent reason for the dark state nature of these compounds.

To observe the phosphorescence emission at room temperature, these compounds were embedded into the PVA matrix to suppress the nonradiative transition and isolate the oxygen to some extent. The obtained films were named **MeTO-1@PVA**, **MeTO-2@PVA**, **MeTO-3@PVA**, and **MeTO-4@PVA**, respectively. Powder X-ray diffraction spectra confirmed the amorphous state of all of the obtained materials (Figure S4). As illustrated in Figure S4, these films exhibited absorption spectra very similar to the same compounds in acetonitrile, except for a little hyperchromatic shift. All of these compounds exhibited distinct emission peaks in the range of 400−700 nm in PL spectra (Figure 3a−d). Specifically, **MeTO-1** exhibited a distinct emission peak around 450 nm and a shoulder peak at around 550 nm in PL spectra, while only a dominant emission peak around 550 nm was observed in delayed spectra (delay time = 0.1 ms, gate time = 2.0 ms). Moreover, the emission lifetimes for the 450 and 550 nm peaks were measured to be 5.96 ns (Figure S6) and 14.08 ms (Figure 3e), respectively. Therefore, the former peak was assigned to a fluorescence emission, and the latter emission was assigned to a phosphorescence emission. The PL and delayed emission spectra of **MeTO-1** in 2-methyl tetrahydrofuran (MTHF) at 77 K could also confirm our conclusions (Figure S7). Similar to **MeTO-1@PVA**, two distinct emission peaks, located at 440 and 518 nm, respectively, were observed for **MeTO-2@PVA** in PL spectra. Combined with the delayed spectra and the PL spectra of **MeTO-2** in MTHF at 77 K, the former peak was assigned to fluorescence emission with a 1.56 ns lifetime, while the latter emission was assigned to phosphorescence emission with an 11.47 ms lifetime. It should be noted that the fluorescence emission of **MeTO-2@PVA** decreased significantly, and the phosphorescence emission evolved into the dominant emission. Almost no fluorescence emission was detected for **MeTO-3@PVA** or **MeTO-4@PVA**. As shown in Figure 3c,d, only strong emission peaks around 470 nm (τ = 11.87 ms) and 450 nm (τ = 3.60 ms) were detected for **MeTO-3@PVA** and **MeTO-4@PVA**, respectively, in the PL spectra. Their delayed emission spectra exhibited a highly similar profile to the PL spectra, which hinted that these materials have almost no fluorescence emission. A similar phenomenon could also be observed in the PL and delayed emission spectra of the same compounds in MTHF at 77 K. The Φ_F and Φ_P values of these compounds exhibited a very interesting variation. As listed in Table 1 and Figure S7, the Φ_F and Φ_P of **MeTO-1@PVA** were estimated to be about 14.6% and 24.0%, respectively, while the Φ_F of **MeTO-2@PVA** significantly decreased to 0.36%, and the Φ_F values of **MeTO-3@PVA** and **MeTO-4@PVA** were estimated to be about 0. The variation of Φ_P was contrary to the Φ_F: a distinct increase was observed, along with a decrease in f (Figure 3f). **MeTO-4@PVA**, which possessed the smallest f, especially showed the highest Φ_P (46.8%) in the PVA matrix. To further confirm the variation of the ratio of fluorescence to phosphorescence and the variation of photoluminescence quantum yield originating from the change of the inherent properties of these molecules with the variation of the substituent position, the emission spectra of these compounds in MTHF at 77 K were examined (Figure S7). Similar to these compounds in the PVA matrix, only compound **MeTO-1** exhibited a distinct fluorescence emission around 420 nm in the PL spectra at 77 K, while **MeTO-2** exhibited a very weak fluorescence emission around 400 nm, and the fluorescence of **MeTO-3** and **MeTO-4** was

https://doi.org/10.1021/jacsau.3c00268
JACS Au 2023, 3, 1835−1842

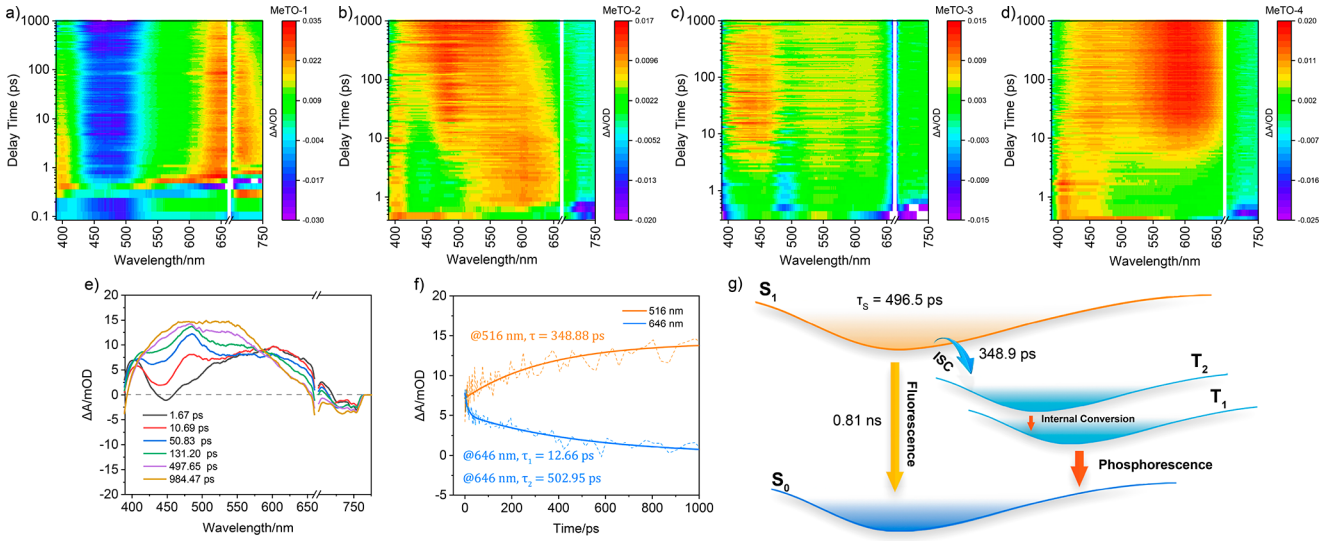

Figure 4. (a–d) Femtosecond broadband-transient absorption spectra of **MeTO**s in acetonitrile under 340 nm excitation. (e) TA spectra of **MeTO-2** at different pump–probe delay times. (f) Dynamics of **MeTO-2** at 516 and 646 nm detection wavelengths (dashed line, experimental data; solid line, fitted results). (g) Jablonski diagram shows the photophysical processes of **MeTO-2** after excitation.

almost undetectable. Using the integral area of the fluorescence and phosphorescence emission peaks of these MTHF solutions in the PL spectra at 77 K, the Φ_{ISC} values were estimated and listed in Table 1. **MeTO-1** exhibited a moderate 63.17% Φ_{ISC}, while a near-unity Φ_{ISC} was estimated for compounds **MeTO-2**, **MeTO-3**, and **MeTO-4**. The k_F values of these compounds in the PVA matrix exhibited a similar variation in acetonitrile (Table 1). The k_F of **MeTO-1** was calculated to be 1.06×10^8 s^{-1}. It decreased by more than an order of magnitude for **MeTO-2**, while the k_F was approximated to be 0 for **MeTO-3** and **MeTO-4**, which both possessed a dark S_1 state because of the near 0 Φ_F values of these compounds.

As mentioned above, a decrease in k_F is an alternative strategy to enhance Φ_{ISC}. To further testify to that point, TDDFT and ORCA calculations were also performed to evaluate the SOC of these compounds. As shown in Figure 3g, the second triplet state (T_2) of these compounds was the highest triplet state less than or close to the S_1 state, and the $S_0 \rightarrow T_1$ and $S_0 \rightarrow T_2$ transitions of these compounds were assigned to $n \rightarrow \pi^*$ or $\pi \rightarrow \pi^*$, respectively. Therefore, either the $S_1 \rightarrow T_1$ or $S_1 \rightarrow T_2$ ISC process will be a spin-allowed process according to the El-Sayed rule,[23] with the $S_1 \rightarrow S_0$ transition configurations of these gradually compounds changed from a $\pi \rightarrow \pi^*$-characterized transition to an $n \rightarrow \pi^*$-characterized transition. ORCA calculations agreed very well with the orbital distribution. Either T_1 or T_2 exhibited a decent SOC value (>6.0 cm^{-1}) with S_1, which provided the probability of efficient RTP. The fluorescence was the dominant emission in the photoluminescence process of **MeTO-1@PVA**, although a large SOC (11.20 cm^{-1}) was calculated between S_1 and T_2, the energy difference between them was as small as 0.028 eV, and the Φ_{ISC} was estimated to be 63.17%. The phosphorescence evolved into the dominant emission for **MeTO-2@PVA**, although the SOC value between its S_1 and T_2 was estimated at only about 6.01 cm^{-1}, despite the similar electron distribution with **MeTO-1**. Moreover, the Φ_{ISC} of **MeTO-2** was estimated to be as high as 98.96% despite the relatively small SOC. This phenomenon indicated that the high SOC value may not be the decisive factor for a high Φ_{ISC}. In consideration of the small k_F of **MeTO-2@PVA**, which was an order of magnitude lower than **MeTO-1@PVA**, we believe the high Φ_{ISC} of **MeTO-2** was the result of the small k_F rather than the SOC. Both the T_1 and T_2 of **MeTO-3** have exhibited a large SOC with S_1, which was estimated to be about 19.79 and 9.10 cm^{-1}, respectively, and the largest SOC (18.18 cm^{-1}) was calculated for **MeTO-4** between T_2 and S_1. With such a large SOC value, the small energy difference between S_1 and T_2 and the forbidden $S_1 \rightarrow S_0$ transition process (extremely small k_F) should be the reasons for the nonfluorescence and strong phosphorescence properties of **MeTO-3** and **MeTO-4** in the PVA matrix at room temperature or MTHF at 77 K.

Femtosecond transient absorption (TA) spectra of these compounds in acetonitrile were measured and are displayed in Figure 4 and Figure S9 to further reveal the photophysical process of these compounds. The absence of the ground-state bleach (GSB) signal of these compounds was due to their absorption being out of our detection range. A strong stimulated emission (SE) signal around 470 nm persisted in the whole detection time window (1000 ps) for **MeTO-1**, and an obvious increase in intensity was observed for it (Figure S9a). Only one excited-state absorption (ESA) in the range of 550–750 nm, assigned to the absorption of the singlet state, was observed right after excitation. The ESA signal exhibited a very slow multiple exponential decay after the excitation. The excitation state did not completely relax to the ground state even after 6000 ps (Figure S9d). No triplet state ESA signal was observed during the experiment, which might result from the signal being too weak to detect or the signal being out of our detection range. We speculated that the ISC process is very slow due to the long-lived singlet state. **MeTO-2** exhibited an ESA signal, assigned to the singlet state absorption, in the range of 500–650 nm right after the excitation and evolved into a long-lived broad ESA band ranging from 400 to 600 nm in 348 ps with the simultaneous decrease of the SE signal around 450 nm (Figure 4b,e). The newly aroused EAS peak was assigned to the absorption of the triplet excited state because the signal kept increasing during the whole detection window. Moreover, the relaxation of the S_1 state and generation of the T_1 state for **MeTO-2** were almost complete at the same time, thereby indicating the near-unity Φ_{ISC} of

https://doi.org/10.1021/jacsau.3c00268
JACS Au 2023, 3, 1835–1842

these compounds (Figure 4f). Figure 4g displays a Jablonski diagram that describes the proposed photophysical behavior of **MeTO-2** after excitation on the basis of the analysis of the TA spectra. Different from compounds **MeTO-1** and **MeTO-2**, no obvious SE or ESA signal was observed for **MeTO-3** right after the excitation, while a broad ESA signal from 400−650 nm evolved in the first 10 ps, which was assigned to the absorption of triplet state (Figure 4c). No obvious decay was observed for the EAS signal during the whole detection window (Figure S9b,e). No appreciable SE signal was observed for **MeTO-4** (Figure 4d, Figure S9c). The almost undetectable SE signal for **MeTO-3** and **MeTO-4** in the TA spectra confirmed the absence of fluorescence of **MeTO-3** and **MeTO-4** in the PL spectra, while an ESA signal around 400−475 nm assigned to the absorption of the singlet state was also recorded for **MeTO-4** right after excitation. The ESA signal evolved into a long-lived broad ESA signal assigned to the triplet state absorption and covered from 400 to 650 nm in 11 ps. The Φ_{ISC} of **MeTO-4** was estimated to be near 100% because of the relaxation of the S_1 state, and the generation of the T_1 state was almost complete at the same time.

In conclusion, a series of efficient RTP materials have been obtained on the basis of the methoxy-substituted thiochroman-4-one skeleton. The fluorescence emission was switched to phosphorescence emission effectively by altering the substituent position of the methoxy group, which is associated with the k_F. The $S_0 \rightarrow S_1$ transition was switched from a bright state to a dark state, which indicated a very small k_F, gradually with the variation of the substituent position. The combination of the small k_F and El-Sayed allowed the ISC process, and the Φ_{ISC} was enhanced from 63.17% to almost 100%, while the Φ_F decreased from 14.6% to about 0%, simultaneously. In line with the enhancement of Φ_{ISC}, the Φ_P values of these compounds were boosted from 24.0% to 46.8%. We demonstrated that decreasing the k_F by rational molecular design is an alternative strategy for efficient organic RTP material. This work provides new insight into the design of the RTP system.

GENERAL PROCEDURE FOR THE FABRICATION OF PVA FILMS

2-Methoxybenzenethiol, 3-methoxybenzenethiol, 4-methoxybenzenethiol, and 3-bromopropanoic acid were purchased from Adamas, Aladdin, or Energy. All solvents were obtained commercially and used as supplied without further purification.

The THF solution of phosphor (5 mL) was added to an aqueous solution (30 mL) of PVA (1.0 g) under vigorous stirring. Then, the solvent was evaporated under a vacuum to obtain the desired phosphor-containing PVA film.

ASSOCIATED CONTENT

Supporting Information

The Supporting Information is available free of charge at https://pubs.acs.org/doi/10.1021/jacsau.3c00268.

Supplemental experimental procedures, 21 figures, and 1 table (PDF)

AUTHOR INFORMATION

Corresponding Author

Xiang Ma − *Key Laboratory for Advanced Materials and Feringa Nobel Prize Scientist Joint Research Center, Frontiers Science Center for Materiobiology and Dynamic Chemistry, School of Chemistry and Molecular Engineering, East China University of Science & Technology, Shanghai 200237, China*; orcid.org/0000-0002-8679-4491; Email: maxiang@ecust.edu.cn

Authors

Liangwei Ma − *Key Laboratory for Advanced Materials and Feringa Nobel Prize Scientist Joint Research Center, Frontiers Science Center for Materiobiology and Dynamic Chemistry, School of Chemistry and Molecular Engineering, East China University of Science & Technology, Shanghai 200237, China*

Yiwei Liu − *Key Laboratory for Advanced Materials and Feringa Nobel Prize Scientist Joint Research Center, Frontiers Science Center for Materiobiology and Dynamic Chemistry, School of Chemistry and Molecular Engineering, East China University of Science & Technology, Shanghai 200237, China*

He Tian − *Key Laboratory for Advanced Materials and Feringa Nobel Prize Scientist Joint Research Center, Frontiers Science Center for Materiobiology and Dynamic Chemistry, School of Chemistry and Molecular Engineering, East China University of Science & Technology, Shanghai 200237, China*; orcid.org/0000-0003-3547-7485

Complete contact information is available at: https://pubs.acs.org/10.1021/jacsau.3c00268

Author Contributions

L.M., H.T., and X.M. conceived this work. L.M. and Y.L. synthesized and characterized the target compounds. All authors participated in the interpretation of data and writing of the manuscript. CRediT: **Liangwei Ma** data curation, investigation, writing-original draft; **Yiwei Liu** investigation; **He Tian** funding acquisition, project administration, resources, supervision; **Xiang Ma** conceptualization, funding acquisition, project administration, resources, supervision, writing-review & editing.

Notes

The authors declare no competing financial interest.

ACKNOWLEDGMENTS

We gratefully acknowledge the financial support from the National Key Research and Development Program of China (2022YFB3203500), NSFC (22125803 and 22020102006), project support by the Shanghai Municipal Science and Technology Major Project (Grant No. 2018SHZDZX03), Program of Shanghai Academic/Technology Research Leader (20XD1421300), China National Postdoctoral Program for Innovative Talents (BX20220106), China Postdoctoral Science Foundation (2022M721140), and Fundamental Research Funds for the Central Universities.

REFERENCES

(1) Li, D.; Lu, F.; Wang, J.; Hu, W.; Cao, X. M.; Ma, X.; Tian, H. Amorphous Metal-Free Room-Temperature Phosphorescent Small Molecules with Multicolor Photoluminescence via a Host-Guest and Dual-Emission Strategy. *J. Am. Chem. Soc.* **2018**, *140* (5), 1916−1923.

(2) Elliott, L. D.; Kayal, S.; George, M. W.; Booker-Milburn, K. Rational Design of Triplet Sensitizers for the Transfer of Excited State Photochemistry from UV to Visible. *J. Am. Chem. Soc.* **2020**, *142* (35), 14947−14956.

(3) Jinnai, K.; Kabe, R.; Lin, Z.; Adachi, C. Organic long-persistent luminescence stimulated by visible light in p-type systems based on organic photoredox catalyst dopants. *Nat. Mater.* **2022**, *21* (3), 338−344.
(4) Lin, F.; Wang, H.; Cao, Y.; Yu, R.; Liang, G.; Huang, H.; Mu, Y.; Yang, Z.; Chi, Z. Stepwise Energy Transfer: Near-Infrared Persistent Luminescence from Doped Polymeric Systems. *Adv. Mater.* **2022**, *34*, 2108333.
(5) Wang, X. F.; Xiao, H.; Chen, P. Z.; Yang, Q. Z.; Chen, B.; Tung, C. H.; Chen, Y. Z.; Wu, L. Z. Pure Organic Room Temperature Phosphorescence from Excited Dimers in Self-Assembled Nanoparticles under Visible and Near-Infrared Irradiation in Water. *J. Am. Chem. Soc.* **2019**, *141* (12), 5045−5050.
(6) Shi, H.; Zou, L.; Huang, K.; Wang, H.; Sun, C.; Wang, S.; Ma, H.; He, Y.; Wang, J.; Yu, H.; Yao, W.; An, Z.; Zhao, Q.; Huang, W. A Highly Efficient Red Metal-free Organic Phosphor for Time-Resolved Luminescence Imaging and Photodynamic Therapy. *ACS Appl. Mater. Interfaces* **2019**, *11* (20), 18103−18110.
(7) Wang, J.; Huang, Z.; Ma, X.; Tian, H. Visible-Light-Excited Room-Temperature Phosphorescence in Water by Cucurbit[8]uril-Mediated Supramolecular Assembly. *Angew. Chem., Int. Ed.* **2020**, *59* (25), 9928−9933.
(8) Zhou, Y.; Qin, W.; Du, C.; Gao, H.; Zhu, F.; Liang, G. Long-Lived Room-Temperature Phosphorescence for Visual and Quantitative Detection of Oxygen. *Angew. Chem., Int. Ed.* **2019**, *58* (35), 12102−12106.
(9) Louis, M.; Thomas, H.; Gmelch, M.; Haft, A.; Fries, F.; Reineke, S. Blue-Light-Absorbing Thin Films Showing Ultralong Room-Temperature Phosphorescence. *Adv. Mater.* **2019**, *31*, 1807887.
(10) Yang, J.; Fang, M.; Li, Z. Stimulus-Responsive Room Temperature Phosphorescence Materials: Internal Mechanism, Design Strategy, and Potential Application. *Acc. Mater. Res.* **2021**, *2*, 644−654.
(11) Cheng, A.; Jiang, Y.; Su, H.; Zhang, B.; Jiang, J.; Wang, T.; Luo, Y.; Zhang, G. Origin of Red-Shifted Phosphorescence from Triphenylamines: Triplet Excimer or Impurity? *Angew. Chem., Int. Ed.* **2022**, *61* (33), e202206366.
(12) Ma, X.; Wang, J.; Tian, H. Assembling-Induced Emission: An Efficient Approach for Amorphous Metal-Free Organic Emitting Materials with Room-Temperature Phosphorescence. *Acc. Chem. Res.* **2019**, *52* (3), 738−748.
(13) Ma, L.; Ma, X. Recent advances in room-temperature phosphorescent materials by manipulating intermolecular interactions. *Sci. China Chem.* **2023**, *66* (2), 304−314.
(14) Kenry; Chen, C.; Liu, B. Enhancing the performance of pure organic room-temperature phosphorescent luminophores. *Nat. Commun.* **2019**, *10* (1), 2111.
(15) Chen, C.; Chi, Z.; Chong, K. C.; Batsanov, A. S.; Yang, Z.; Mao, Z.; Yang, Z.; Liu, B. Carbazole isomers induce ultralong organic phosphorescence. *Nat. Mater.* **2021**, *20* (2), 175−180.
(16) Kabe, R.; Adachi, C. Organic long persistent luminescence. *Nature* **2017**, *550* (7676), 384−387.
(17) Gao, H.; Ma, X. Recent progress on pure organic room temperature phosphorescent polymers. *Aggregate* **2021**, *2* (4), e38.
(18) Cheng, Z.; Shi, H.; Ma, H.; Bian, L.; Wu, Q.; Gu, L.; Cai, S.; Wang, X.; Xiong, W.-w.; An, Z.; Huang, W. Ultralong Phosphorescence from Organic Ionic Crystals under Ambient Conditions. *Angew. Chem., Int. Ed.* **2018**, *57* (3), 678−682.
(19) Zhang, Z.-Y.; Liu, Y. Ultralong room-temperature phosphorescence of a solid-state supramolecule between phenylmethylpyridinium and cucurbit[6]uril. *Chem. Sci.* **2019**, *10* (33), 7773−7778.
(20) Yang, Z.; Xu, C.; Li, W.; Mao, Z.; Ge, X.; Huang, Q.; Deng, H.; Zhao, J.; Gu, F. L.; Zhang, Y.; Chi, Z. Boosting the Quantum Efficiency of Ultralong Organic Phosphorescence up to 52% via Intramolecular Halogen Bonding. *Angew. Chem., Int. Ed.* **2020**, *59* (40), 17451−17455.
(21) Wang, Q.; Dou, X.; Chen, X.; Zhao, Z.; Wang, S.; Wang, Y.; Sui, K.; Tan, Y.; Gong, Y.; Zhang, Y.; Yuan, W. Z. Reevaluating Protein Photoluminescence: Remarkable Visible Luminescence upon Concentration and Insight into the Emission Mechanism. *Angew. Chem., Int. Ed.* **2019**, *58* (36), 12667−12673.
(22) Wang, G.; Wang, Z.; Ding, B.; Ma, X. pH-Responsive amorphous room-temperature phosphorescence polymer featuring delayed fluorescence based on fluorescein. *Chin. Chem. Lett.* **2021**, *32*, 3039−3042.
(23) El-Sayed, M. A. Spin—Orbit Coupling and the Radiationless Processes in Nitrogen Heterocyclics. *J. Chem. Phys.* **1963**, *38* (12), 2834−2838.
(24) An, Z.; Zheng, C.; Tao, Y.; Chen, R.; Shi, H.; Chen, T.; Wang, Z.; Li, H.; Deng, R.; Liu, X.; Huang, W. Stabilizing triplet excited states for ultralong organic phosphorescence. *Nat. Mater.* **2015**, *14* (7), 685−690.
(25) Ding, B.; Ma, L.; Huang, Z.; Ma, X.; Tian, H. Engendering persistent organic room temperature phosphorescence by trace ingredient incorporation. *Sci. Adv.* **2021**, *7* (19), eabf9668.
(26) Sun, S.; Wang, J.; Ma, L.; Ma, X.; Tian, H. A Universal Strategy for Organic Fluid Phosphorescence Materials. *Angew. Chem., Int. Ed.* **2021**, *60* (34), 18557−18560.
(27) Wang, Z.; Cheng, X.; Xie, Y.; Liu, S.; Dong, M.; Zhao, J.; Liang, F.; An, Z.; Huang, W. Recent Advances in Organic Room-Temperature Phosphorescence of Heteroatom (B/S/P)-Containing Chromophores. *CCS Chem.* **2023**, *5* (2), 292−309.
(28) Sun, S.; Ma, L.; Wang, J.; Ma, X.; Tian, H. Red-light excited efficient metal-free near-infrared room-temperature phosphorescent films. *Natl. Sci. Rev.* **2022**, *9* (2), nwab085.
(29) Ma, X. K.; Zhang, W.; Liu, Z.; Zhang, H.; Zhang, B.; Liu, Y. Supramolecular Pins with Ultralong Efficient Phosphorescence. *Adv. Mater.* **2021**, *33* (14), 2007476.
(30) Wang, J.; Dang, Q.; Gong, Y.; Liao, Q.; Song, G.; Li, Q.; Li, Z. Precise Regulation of Distance between Associated Pyrene Units and Control of Emission Energy and Kinetics in Solid State. *CCS Chem.* **2021**, *3* (12), 274−286.
(31) Huang, A.; Li, Q.; Li, Z. Molecular Uniting Set Identified Characteristic (MUSIC) of Organic Optoelectronic Material. *Chin. J. Chem.* **2022**, *40* (19), 2356−2370.
(32) Li, H.; Kim, H.; Han, J.; Nguyen, V. N.; Peng, X.; Yoon, J. Activity-based smart AIEgens for detection, bioimaging, and therapeutics: Recent progress and outlook. *Aggregate* **2021**, *2* (4), e51.
(33) Duo, Y.; Luo, G.; Zhang, W.; Wang, R.; Xiao, G. G.; Li, Z.; Li, X.; Chen, M.; Yoon, J.; Tang, B. Z. Noncancerous disease-targeting AIEgens. *Chem. Soc. Rev.* **2023**, *52* (3), 1024−1067.
(34) Kumar, V.; Kim, H.; Pandey, B.; James, T. D.; Yoon, J.; Anslyn, E. V. Recent advances in fluorescent and colorimetric chemosensors for the detection of chemical warfare agents: a legacy of the 21st century. *Chem. Soc. Rev.* **2023**, *52* (2), 663−704.
(35) Teng, K. X.; Niu, L. Y.; Yang, Q. Z. Supramolecular Photosensitizer Enables Oxygen-Independent Generation of Hydroxyl Radicals for Photodynamic Therapy. *J. Am. Chem. Soc.* **2023**, *145*, 4081−4087.
(36) Chen, Y.; Wang, S.; Zhang, F. Near-infrared luminescence high-contrast in vivo biomedical imaging. *Nat. Rev. Bioeng.* **2023**, *1* (1), 60−78.
(37) Lewis, G. N.; Kasha, M. Phosphorescence and the Triplet State. *J. Am. Chem. Soc.* **1944**, *66* (12), 2100−2116.
(38) Zhao, W.; Cheung, T. S.; Jiang, N.; Huang, W.; Lam, J. W. Y.; Zhang, X.; He, Z.; Tang, B. Z. Boosting the efficiency of organic persistent room-temperature phosphorescence by intramolecular triplet-triplet energy transfer. *Nat. Commun.* **2019**, *10* (1), 1595.
(39) Huang, L.; Chen, B.; Zhang, X.; Liao, F.; Miao, H.; Luo, Y.; Zhang, G.; Trindle, C. O.; Wang, Y. Proton-Activated "Off-On" Room-Temperature Phosphorescence from Purely Organic Thioethers. *Angew. Chem., Int. Ed.* **2018**, *57* (49), 16046−16050.
(40) Kuila, S.; Rao, K. V.; Garain, S.; Samanta, P. K.; Das, S.; Pati, S. K.; Eswaramoorthy, M.; George, S. J. Aqueous Phase Phosphorescence: Ambient Triplet Harvesting of Purely Organic Phosphors via Supramolecular Scaffolding. *Angew. Chem., Int. Ed.* **2018**, *57* (52), 17115−17119.

https://doi.org/10.1021/jacsau.3c00268
JACS Au 2023, 3, 1835−1842

(41) Chen, H.; Yao, X.; Ma, X.; Tian, H. Amorphous, Efficient, Room-Temperature Phosphorescent Metal-Free Polymers and Their Applications as Encryption Ink. *Adv. Optical Mater.* **2016**, *4* (9), 1397−1401.
(42) Yan, Z. A.; Lin, X.; Sun, S.; Ma, X.; Tian, H. Activating Room-Temperature Phosphorescence of Organic Luminophores via External Heavy-Atom Effect and Rigidity of Ionic Polymer Matrix*. *Angew. Chem., Int. Ed.* **2021**, *60* (36), 19735−19739.
(43) Tian, S.; Ma, H.; Wang, X.; Lv, A.; Shi, H.; Geng, Y.; Li, J.; Liang, F.; Su, Z. M.; An, Z.; Huang, W. Utilizing d-ppi Bonds for Ultralong Organic Phosphorescence. *Angew. Chem., Int. Ed.* **2019**, *58* (20), 6645−6649.
(44) Wang, T.; Gupta, A. K.; Wu, S.; Slawin, A. M. Z.; Zysman-Colman, E. Conjugation-Modulated Excitonic Coupling Brightens Multiple Triplet Excited States. *J. Am. Chem. Soc.* **2023**, *145* (3), 1945−1954.
(45) Ma, L.; Ding, B.; Yuan, Z.; Ma, X.; Tian, H. Triboluminescence and Selective Hydrogen-Bond Responsiveness of Thiochromanone Derivative. *ACS Mater. Lett.* **2021**, 3, 1300−1306.
(46) Brühlmann, U.; Serafimov, O.; Huber, J. R. Excited State Behavior of Aromatic Amines in Solution: Dihydrophenazine Derivatives. *Berichte der Bunsengesellschaft für physikalische Chemie* **1975**, *78* (12), 1348−1353.
(47) Ma, L.; Sun, S.; Ding, B.; Ma, X.; Tian, H. Highly Efficient Room-Temperature Phosphorescence Based on Single-Benzene Structure Molecules and Photoactivated Luminescence with Afterglow. *Adv. Funct. Mater.* **2021**, *31* (17), 2010659.
(48) Lu, T.; Chen, F. Multiwfn: A multifunctional wavefunction analyzer. *J. Comput. Chem.* **2012**, *33* (5), 580−592.

https://doi.org/10.1021/jacsau.3c00268
JACS Au 2023, 3, 1835−1842